

Relationship Between Mirror Dimensions and Failure Stress for Optical Fibers

Robert J. Castilone, G. Scott Glaesemann, Thomas A. Hanson*
Corning Incorporated, Corning, NY 14830

ABSTRACT

Standard glass optical fiber was intentionally damaged and strength tested in tension for a wide range of failure stress values. The mirror/mist boundary on each specimen was measured and compared to the measured failure stress. When the size of the fracture mirror is small compared to the fiber diameter, the well-known linear square root dependence of strength on mirror size was reaffirmed. However, when the mirror size approaches the fiber diameter, this relationship does not hold. The classical relationship overestimates the failure stress for large mirrors. It was determined that the circular shape of the fiber contributes to, but can not fully account for, departure from the classical strength/mirror relationship. A new empirical relationship was developed to enable predictive determinations of failure stress to levels as low as 20 to 25 kpsi (0.14 to 0.17 GPa).

1. INTRODUCTION

The study of fracture surface markings on glass, including optical fibers, has been well documented. During failure, the crack front propagates through the material, creating fracture features known as the mirror, mist, and hackle. The crack front initially produces the smooth mirror region. However, as the crack accelerates it becomes more unstable, creating a dimpled surface known as mist. This instability eventually causes the crack to branch out, producing the rough hackle region. The hackle region is characterized by elongated markings that proceed in the direction of crack propagation. The hackle markings point back to the flaw origin.¹

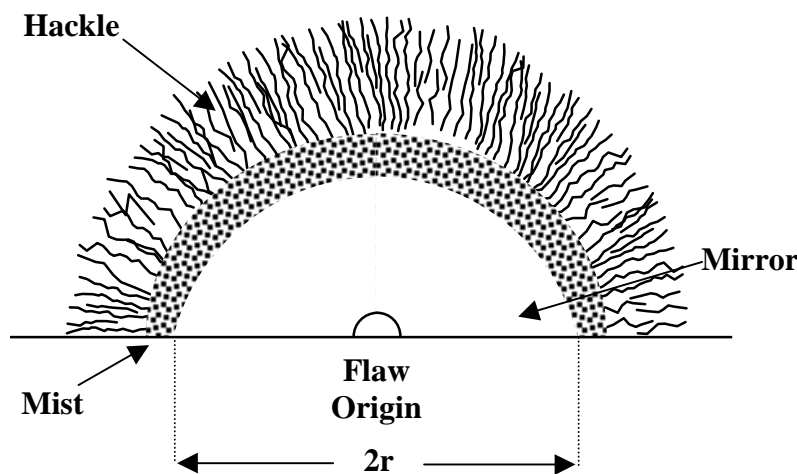


Figure 1. Schematic showing typical glass surface features that form during failure.

* email correspondence: castilonrj@corning.com, glaesemags@corning.com, hansonta@corning.com

Numerous studies have indicated a relationship between the specimen failure stress and the dimensions of the mirror region. These studies have shown the mirror radius, r , to relate to failure stress, σ , through the square root dependence shown in Eq. (1),^{2,3}

$$\sigma = \frac{A}{\sqrt{r}} \quad (1)$$

where A represents the mirror constant for the material. Typically, the mirror size is measured at the intersecting points where the mist meets the material surface, as indicated by $2r$ in Figure 1. The mirror constant, A , is empirically determined by a regression of strength and mirror measurement data. In a recent review paper on fiber fracture surface analysis, Mecholsky⁴ presented data showing that Eq. (1) is valid for a wide range of stresses and mirror dimensions. A mirror constant of $2.1 \text{ MPa}\cdot\text{m}^{1/2}$ ($305 \text{ kpsi}\cdot\mu\text{m}^{1/2}$) was found to fit the data, which ranged from 100 to 2000 MPa (roughly 10 - 300 kpsi). The data showed similar results for bulk fused silica and for silica fibers over this wide range of strengths. However, there is some uncertainty in A due to the limited number samples.

Several considerations and recommendations for utilizing the mirror dimensions to estimate the failure stress can be found in literature. For example;

- Ensure that the measurement procedures are consistent with those used during the development of the mirror constant.⁵
- Sufficient magnification need be used to adequately determine the onset of mist.⁶
- Forces resulting from residual stress and bending can alter the mirror shape.^{2,7}
- Fibers with high density cores can alter the mirror shape.⁸
- Measurements along the free boundary surface should be avoided, due to the possibility that surface damage artifacts distort the mirror.⁵ Rather, mirror measurements should be taken several microns away from the specimen surface.
- The mirror dimensions should be small relative to the specimen.²

The last admonition is particularly difficult for optical fiber, as the failure stress when the mirror is near the size of the fiber is particularly important from a reliability point of view. For example, after processing or installation, a fiber is found to be broken and the fracture surface shows primarily mirror with a trace of mist. Quantifying the failure stress in this case is critical to determining the location and root cause of the failure event. This study examines the mirror-failure stress relationship for a wide range of mirror dimensions on optical fiber, especially where the mirrors are of the size of the fiber. Indeed it will be shown that Eq. (1) is not appropriate for large mirrors. A method for estimating fiber failure stress for large mirrors will be established. In particular, the circular shape of the fiber can be and should be accounted for when mirrors are large.

2. METHOD FOR CREATING STRENGTH AND MIRROR DATA ON OPTICAL FIBER

In order to obtain mirror sizes in the range of interest, flaws were intentionally introduced onto the fiber surface. The fiber used was a step index single-mode fiber. Initially $125 \mu\text{m}$ glass-diameter fiber was measured; however, as the experiment evolved $80 \mu\text{m}$, $154 \mu\text{m}$, and $180 \mu\text{m}$ diameter fibers were also tested. The fibers were initially stripped of their coating using methylene chloride. With the coating removed, several techniques were used to create the flaws. One technique involved dropping silicon carbide particles (SiC) onto the glass surface. To create a range of flaws, varying grit sizes and quantities of SiC were used. Other methods of inducing flaws included using a cleaver blade and a scribe.

Once the flaws were created, the fiber specimens were immediately strength tested on a universal-testing machine.^α The fiber region containing the flaw was placed within the gauge length and pulled to failure in pure tension. The strength

^α Instron Corp., Canton, MA

tests were conducted with varying stressing rates, utilizing fatigue as another way to create different mirror sizes. Although fatigue has a direct influence on subcritical crack growth and the size of the flaw when it reaches K_{IC} , the formation of the mirror is not influenced by such subcritical growth.⁵ Also, fatigue prior to failure will mitigate the effects of contact residual stress on the resulting mirror-failure stress relationship. The break force was recorded during failure and the two break ends were collected for mirror measurement.

The break ends were examined with a polarized-light optical microscope. The microscope was equipped with a Nomarski-modified Wallaston prism to aid in the determination of the fractographic features. The measurements were made in reflected light using an eyepiece reticle. The reticle was calibrated using a known measurement standard. To minimize error, each reticle measurement was verified using a video measurement system. Measurements were made using 500 and 1000 times magnification depending on the mirror size.

For each break, the mirror radius was measured in two ways, as shown in Figure 2. The method espoused in literature is where one takes the mirror radius, r_w , to be half the width of intersecting points of the mirror/mist boundary with the surface of the specimen. Note that due to the curvature of optical fiber surfaces, the line connecting these intersecting points does not travel through the failure origin. The second mirror measurement technique is where one measures from the failure origin directly across to the apex of the mirror. For the purposes of this paper, this measurement is denoted as the mirror radius-depth, r_d .

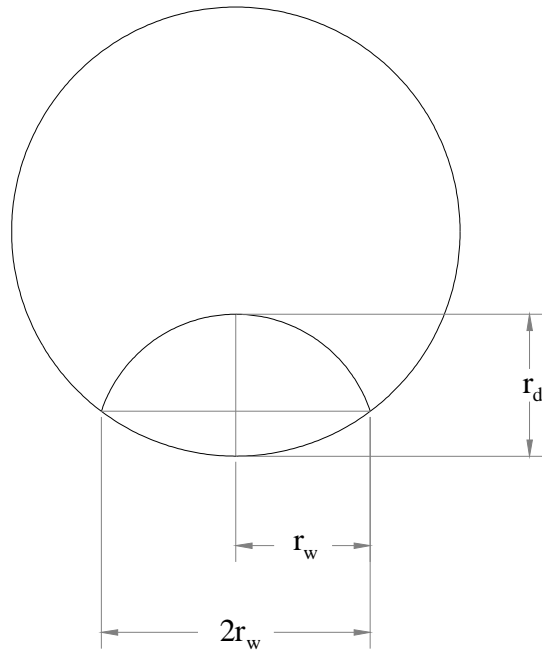


Figure 2. Schematic showing mirror radius-depth (r_d) and radius-width (r_w) measurements on a fiber break end.

3. RESULTS & DISCUSSION

1. Analyzing the Strength and Mirror Measurement Data

Figure 3 shows the relationship between the mirror dimensions and the measured failure stress for 125 micron fiber. Both the mirror radius-width, r_w , and radius-depth, r_d , measurement results are shown. The radius-depth values follow a square root dependence with the failure stress. The corresponding mirror constant, A_d , of $265 \text{ kpsi} \cdot \mu\text{m}^{1/2}$ ($1.83 \text{ MPa} \cdot \text{m}^{1/2}$) was calculated. For small mirrors, the radius-width, r_w , values show the same relationship as the depth measurement. However, as the mirror approaches the size of the fiber, the radius-width values clearly deviate from the

square root relationship. This demonstrates the validity of the historical admonition of being cautious when mirrors are of the size of the specimen. With 125 μm fiber, Eq. (1) should not be used for r_w values larger than 30 μm .

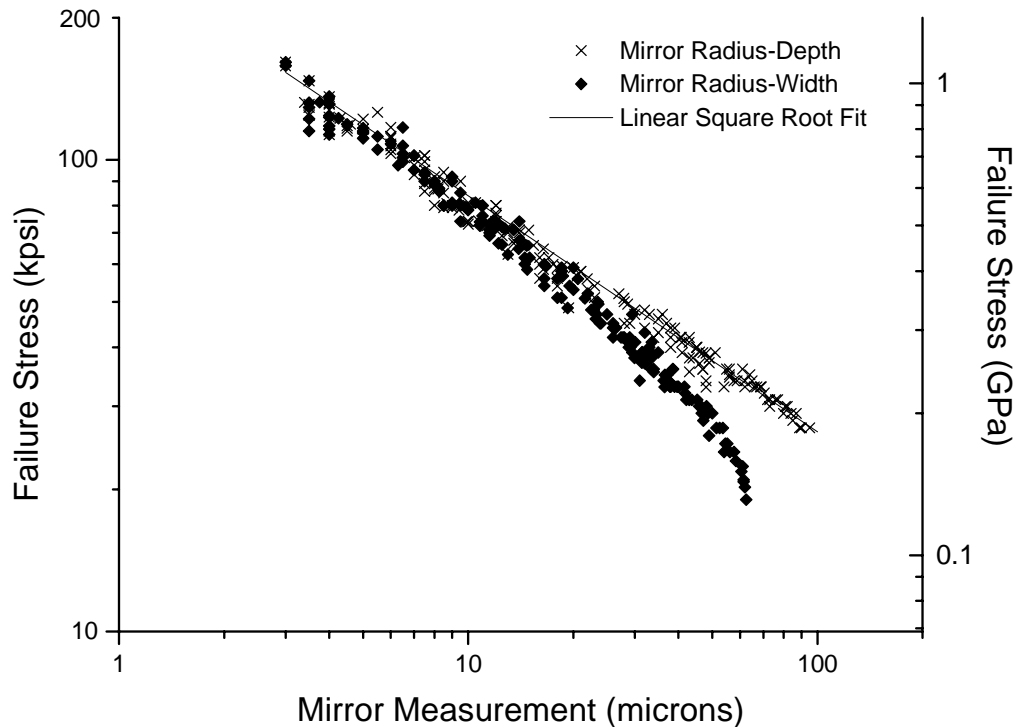
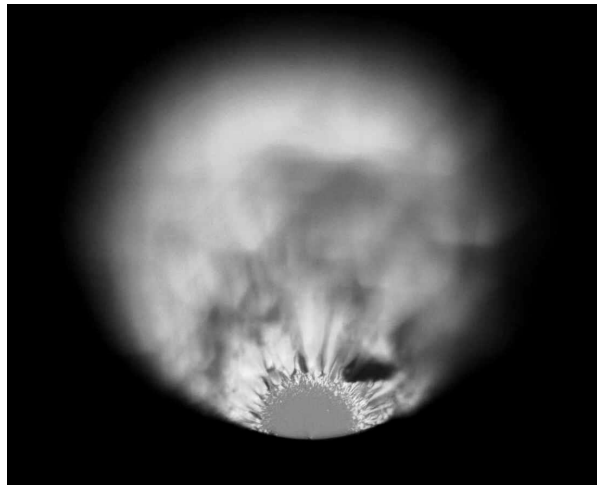


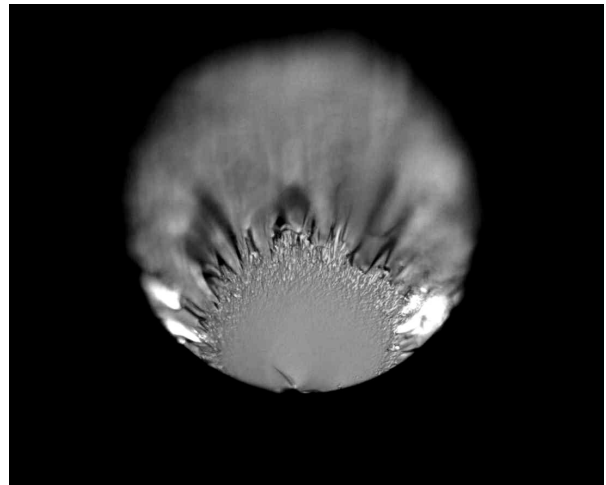
Figure 3. Plot showing the mirror radius-depth (r_d) and radius-width (r_w) measurement values versus failure stress for 125 μm diameter fiber.

Figure 4 shows fracture surface images for ever decreasing strengths. In Image A the mirror is well contained within the fracture surface and the normal progression through mirror, mist, and mist-hackle is evident. The width and depth mirror dimensions are similar for this size mirror. As the mirror becomes a larger portion of the fracture surface, at lower failure stress levels, several fracture surface features can be observed. In Image D the crack front transitions from mist-hackle back to mist and then finally to mirror near the furthest edge away from the origin (see arrow). This indicates that the crack front decelerated by encountering lower stress just before final glass separation. It is typically assumed that bending is present when a crack front transitions from mist-hackle back to mirror as in Image D.^β At the lower stress level of 27 kpsi in Image E the crack front reaches a velocity across the depth sufficient only to form mist before decelerating back to mirror as in Image D. At 21 kpsi in Image F the mirror appears to extend across the entire depth of the fracture surface. Notice that mist and hackle still form at the outermost width of the mirror on these specimens in Images E and F, suggesting either a higher crack front velocity or greater instability in that region. Shand⁵ noted that surface defects can destabilize the crack front enough to create mist and hackle. However, this isn't the case for these optical fiber specimens because their surface is pristine away from the fracture origin. Thus, it is believed that the mist and hackle that remain in this region are simply due to higher stress. This is important, as these markings are needed in the estimation of the remote applied stress at failure. At stress levels below 21 to 25 kpsi (0.14 to 0.17 GPa) there is only a mirrored surface for 125 micron diameter fiber and the crack front never reaches velocities sufficient to create mist.

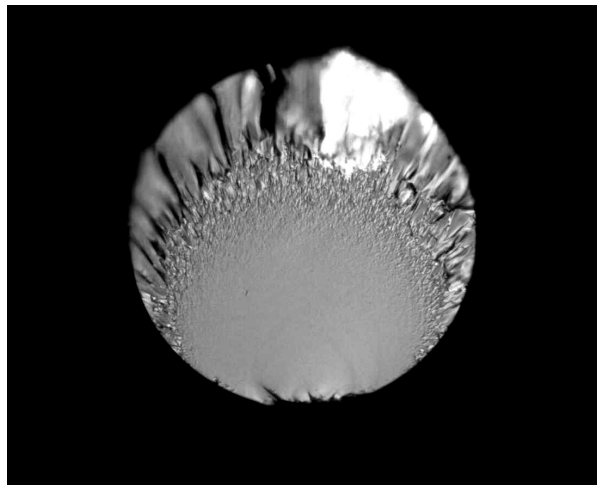
^β Fiber failures in a constrained condition show the same fracture surface features as those shown in Images D and E. It is believed that if bending is present, it is generated during the fracture event itself. Along with other speculations, a shift in the neutral axis of the fiber during fast fracture could be a source of bending. A brief literature review revealed little discussion on the matter. The generation of bend stress during fracture of specimens tested in tension would be of considerable practical interest for interpreting fractographic evidence from processing and field failures of optical fiber.



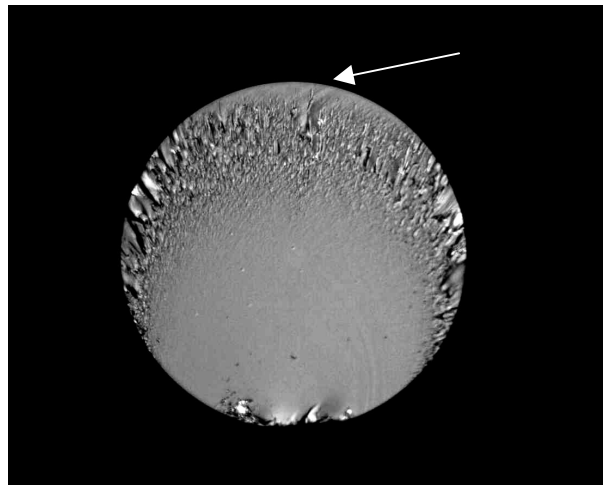
A) 78 kpsi



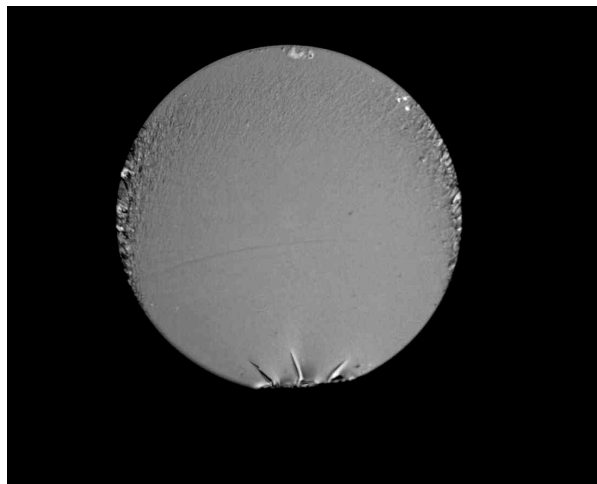
B) 47 kpsi



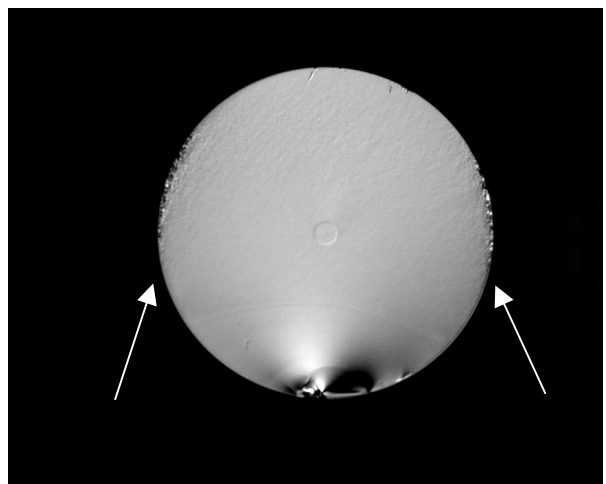
C) 36 kpsi



D) 31 kpsi - arrow shows reformation of mirror region



E) 27 kpsi



F) 21 kpsi - arrows show mist region

Figure 4. Optical microscope images showing fracture surfaces for various break stress values.

When the mirror becomes the size of the specimen, the width of the mirror is interrupted by the curvature of a circular object like fiber. This is shown schematically in Figure 5. The dimension r_x represents a continuation of the circular mirror to a plane even with the origin and is related to the mirror width measurement, r_w , by

$$r_x = \sqrt{r_w^2 + \left(R_f - \sqrt{R_f^2 - r_w^2} \right)^2} \quad (2)$$

where R_f is the fiber radius. The extended mirror dimension, r_x , was calculated for each specimen in Figure 3 and is plotted in Figure 6. With the extended values, much of the non-linearity observed in the width measurement is removed, especially with the largest mirrors. However, some curvature in the data still remains at lower stress levels.

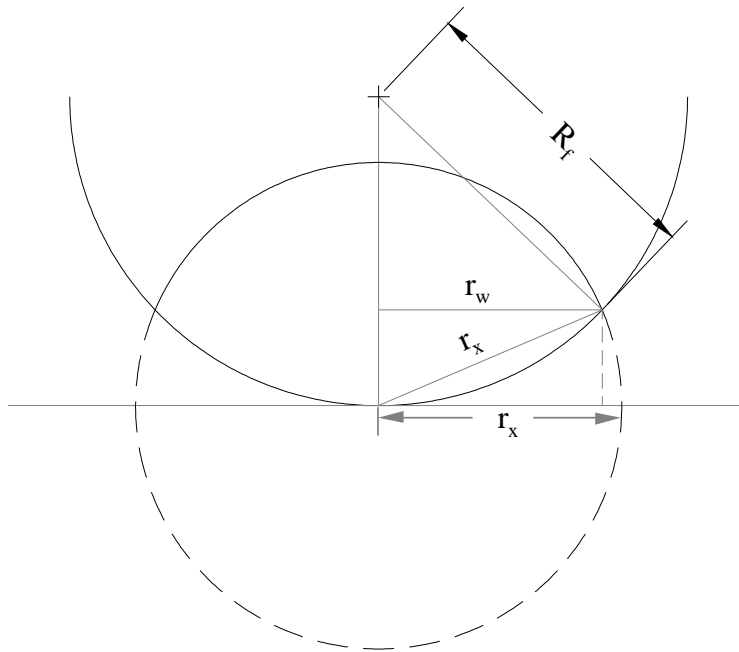


Figure 5. Schematic showing the extended radius-width measurement (r_x) and a fiber of radius (R_f).

To further understand the behavior of the mirror in relation to the circularity of the fiber, an experiment similar to that above was carried out on 80, 154, and 180 μm diameter fibers. Figure 7 shows the radius-depth, r_d , data for these fibers while Figure 8 shows the radius-width, r_w , data. With the radius-depth measurement, all the data displays the same square root dependence, regardless of the fiber diameter.⁸ The radius-width results in Figure 8, just like the 125 micron fiber, show a non-linear dependence of \log (failure stress) with \log (mirror width). Upon close examination of the data in Figure 8 one observes this non-linearity to be more pronounced for smaller diameter fibers. Conversely, as the fiber becomes less circular the mirror approaches the traditional square root dependence found in rectangular bulk specimens. The significance of this observation becomes clear when the strength results in Figure 8 are replotted in Figure 9 with the extended mirror radius, r_x , from Eq. (2). Using the extended mirror, r_x , the data from all four fiber diameters lie on a single curve. Thus, when the mirror is close to the size of the specimen the dimensions of the specimen can affect the actual mirror measurement. Moreover, for circular specimens, one can account for this effect and obtain meaningful failure stress predictions down to low stress levels.

⁸ This is interesting, but lacks practical importance as the mirror in this direction (radius-depth) is distorted in applications where bending is present. Furthermore, the width measurement allows one to obtain measurements down to significantly lower failure stress levels.

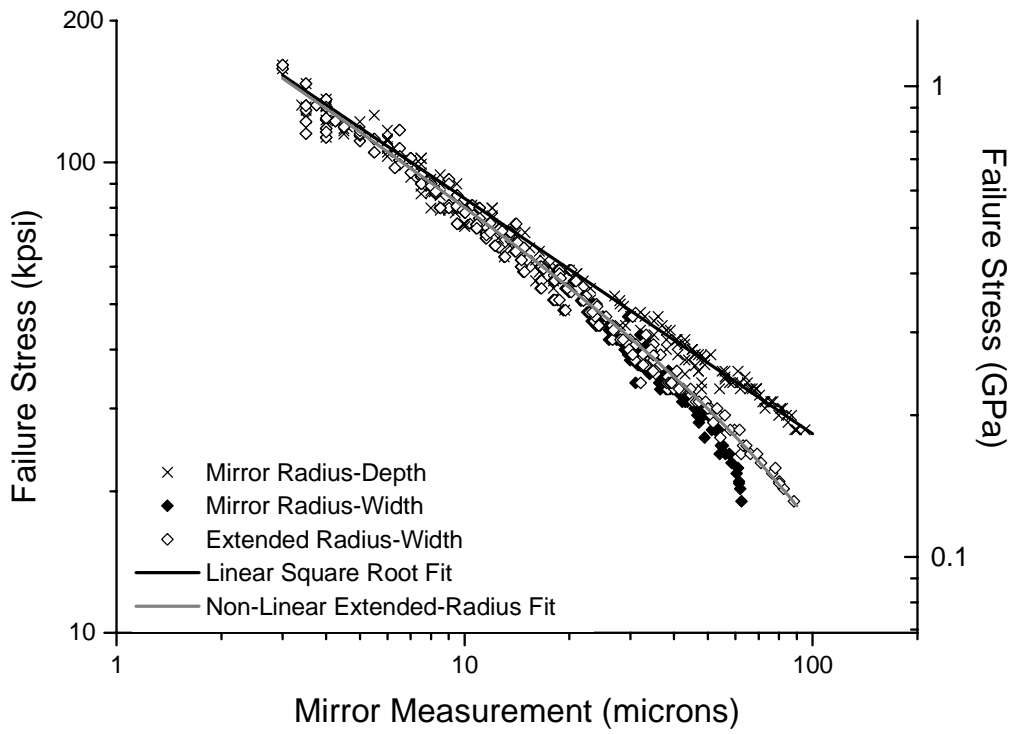


Figure 6. Plot showing mirror measurement values versus failure stress including the extended radius-width (r_x) data.

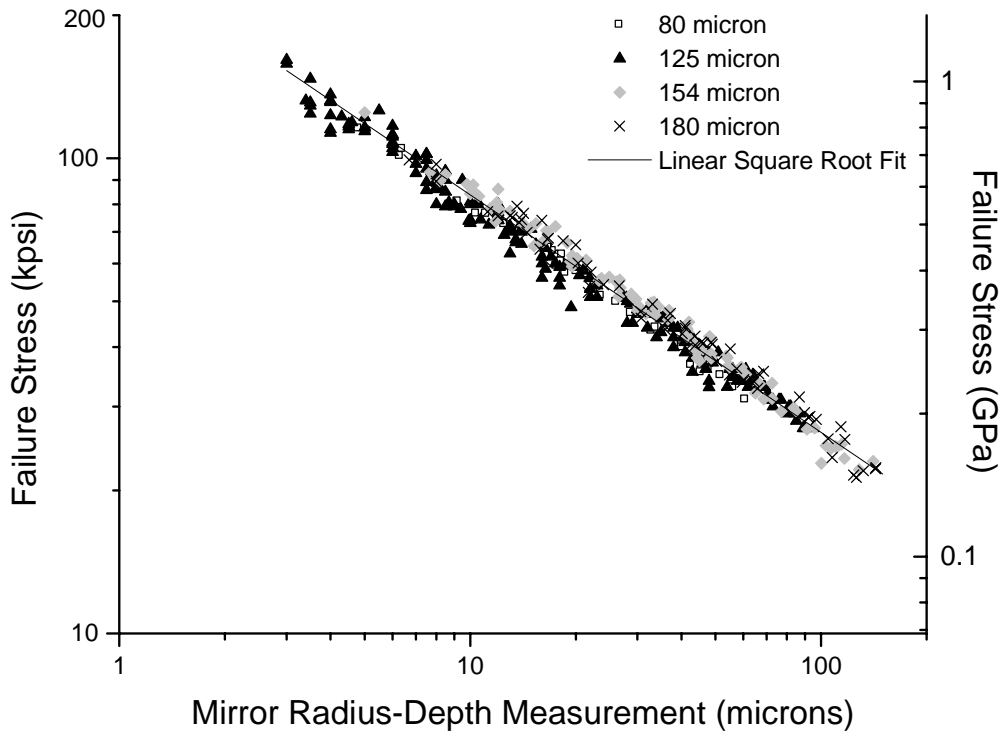


Figure 7. Plot showing mirror radius-depth (r_d) measurement values versus failure stress for various diameter fibers.

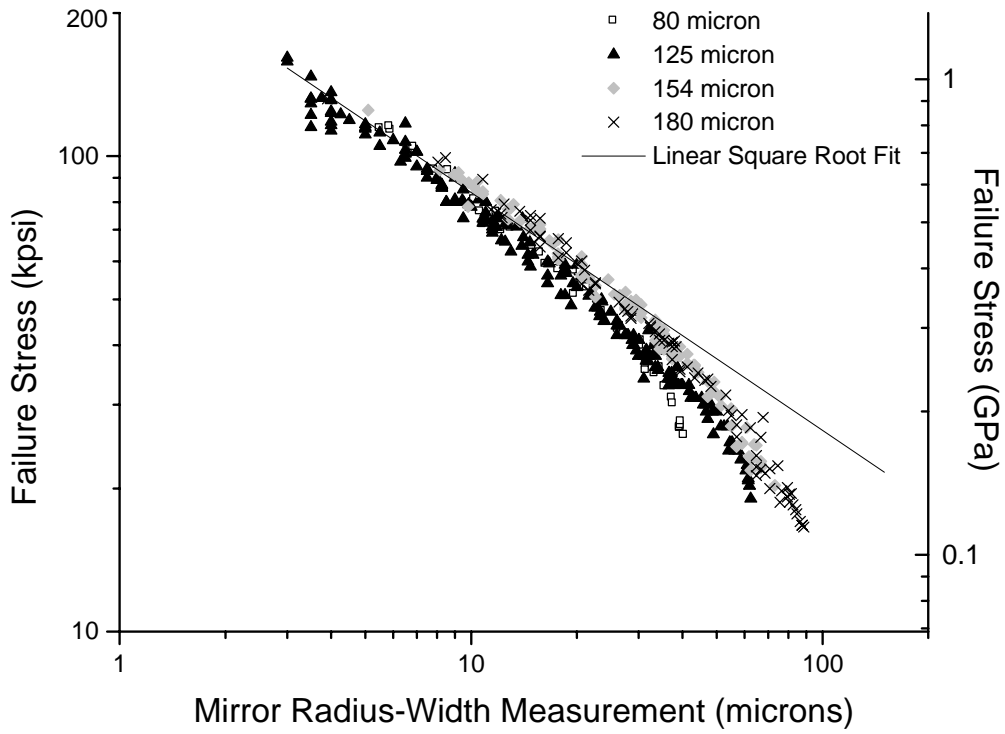


Figure 8. Plot showing mirror radius-width (r_w) measurement values versus failure stress for various diameter fibers.

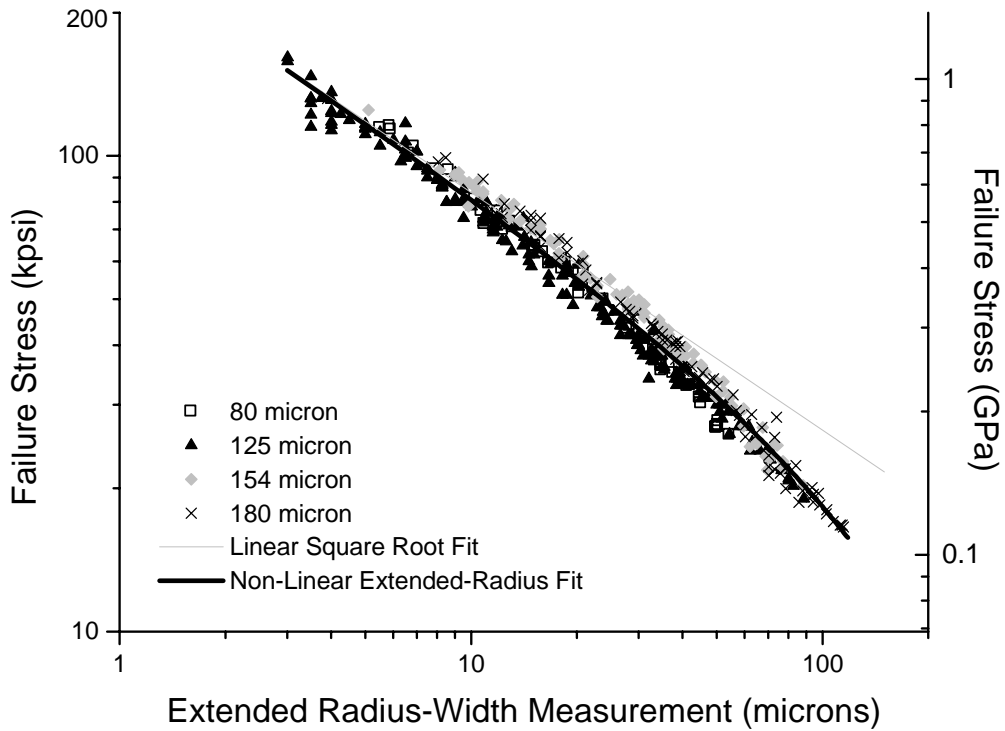


Figure 9. Plot showing extended radius-width (r_x) measurement values versus failure stress for various diameter fibers.

2. Empirical Failure Stress Predictions from Mirror Measurements

The square root dependence in Eq. (1) has ties to fracture mechanics where strength is similarly related to flaw size. It is clear from the results of this study that this form is not suitable when working with large mirrors. An empirical relationship was created by adding a term to Eq. (1),

$$\sigma = \frac{A}{\sqrt{r_x \cdot \exp(B \cdot r_x)}} \quad (3)$$

where r_x is the extended radius-width from Eq. (2), and B is the non-linear mirror factor. The mirror constant A was determined from the strength and mirror data from the high strength region, where the mirror is small compared to the fiber diameters, as $A = 265 \text{ kpsi} \cdot \mu\text{m}^{1/2}$ ($1.83 \text{ MPa} \cdot \text{m}^{1/2}$). A regression of strength and mirror data from all four fiber diameters in Figure 9 yielded a B value of $7.4 \times 10^{-3} \mu\text{m}^{-1}$ ($7.4 \times 10^3 \text{ m}^{-1}$). The results from this analysis are shown in Figure 9 to give a reasonable representation of failure stress as a function of mirror radius for a wide range of failure stresses and fiber diameters.

4. CONCLUSIONS

Standard 125 μm glass optical fiber was intentionally damaged and strength tested in tension for a wide range of failure stress values. The mirror/mist boundary on each specimen was measured and compared to the measured failure stress. When the size of the fracture mirror was small compared to the fiber diameter, the well-known linear square root dependence of strength on mirror size was reaffirmed. A mirror constant of $265 \text{ kpsi} \cdot \mu\text{m}^{1/2}$ was determined. In keeping with historical caution, when the mirror is of the size of the fiber diameter it was shown that this relationship does not hold. The classical relationship overestimates the failure stress when the mirror size approaches the fiber diameter. In this extreme case the circular shape of the fiber plays an increasing role. Fibers with diameters ranging from 80 μm to 180 μm were tested in the same fashion and were found to exhibit similar behavior. However, the departure from the classic relationship was more pronounced for the smaller diameter fibers. Assuming mirror formation to be interrupted by the curved fiber surface, the mirror was extended to the same plane as the failure origin. This extended mirror radius was calculated for all specimens resulting in a universal curve for the range of fiber diameters tested in this study. Even with the use of an extended mirror radius, there is still some departure from the classical strength/mirror radius relationship when the mirror is large. An empirical relationship was developed to enable predictive determinations of failure stress to levels as low as 20 to 25 kpsi (0.14 to 0.17 GPa), where the fracture surface becomes full-mirrored.

There are several practical implications one can deduce from this study. First, there is a practical need for making failure stress predictions from fiber failures with large mirrors. This can now be done with greater confidence. Second, researchers attempting to correlate fractographic dimensions to physical properties should heed the historical admonition to avoid large mirrors. However, note that a failure stress/mirror size relationship does exist, even in this extreme, and perhaps it can be used to further understand the fundamental physics of fracture. Finally, specialty fiber applications employ the use of non-standard fiber diameters. This study shows that the influence of glass diameter on the formation of large mirrors can be accounted for.

5. ACKNOWLEDGMENTS

The authors would like to thank everyone involved in the measurement and data analysis for this paper: Chris Barnett, Brenda Christian, Don Clark, Steve DeMartino, Phil Gleason, Marcia Gray, Tim Jackson, and Jamie Westbrook. A special thank-you to Dan Hill.

6. REFERENCES

1. V. Frechette, *Failure Analyses of Brittle Material; Advances in Ceramics – Volume 28*, The American Ceramic Society, Westerville, Ohio, 1990.
2. E. B. Shand, “Breaking Stress of Glass Determined from Dimension of Fracture Mirrors,” *J of Amer. Ceram. Soc.* **42** [10], pp. 474-477, 1959.
3. J. J. Mecholsky, R. W. Rice, and S. W. Freiman, “Prediction of Fracture Energy and Flaw Size in Glasses from Measurements of Mirror Size,” *J of Amer. Ceram. Soc.* **57** [10], pp. 440-443, 1973.
4. J. J. Mecholsky, “Fracture Surface Analysis of Optical Fibers,” *Ceramics and Glasses of the Engineered Materials Handbook, Vol. 4*, pp. 663-668, ASM International, 1991.
5. E. B. Shand, “Breaking Stress of Glass Determined from Fracture Surfaces,” *The Glass Industry*, pp. 190-194, 1967.
6. T. A. Michalske, “Quantitative Fracture Surface Analysis,” *Ceramics and Glasses of the Engineered Materials Handbook, Vol. 4*, pp. 652-662, ASM International, 1991.
7. D. G. Holloway, “The Fracture Behavior of Glass,” *Glass Technology* **27** [4], pp. 120-133, 1986.
8. J. E. Field, B. Samuels, D. Townsend, and J. T. Hagan, “Cleavage of optical fibers following diamond-wedge indentation,” *Philosophical Magazine*, **57** [2], pp. 151-171, 1998.